Stable Mg 2+ Dication Weakly Stabilized/Coordinated in Solution: Synthesis, Structure, Reactivity, and Use in Catalysis

Xuejuan Xu, Alain Chaumont, Christophe Gourlaouen, Satawat Tongdee, Sandip Munshi, Béatrice Jacques, Rudolf Wehmschulte, Samuel Dagorne

How to cite: *Angew. Chem. Int. Ed.* **2025**, *64*, e202506266
doi.org/10.1002/anie.202506266

Electrophilic Species

Stable Mg^{2+} Dication Weakly Stabilized/Coordinated in Solution: Synthesis, Structure, Reactivity, and Use in Catalysis

Xuejuan Xu, Alain Chaumont, Christophe Gourlaouen, Satawat Tongdee, Sandip Munshi, Béatrice Jacques, Rudolf Wehmschulte, and Samuel Dagorne**

Abstract: The first soluble and stable Mg^{2+} dication stabilized only by weakly coordinating and chemically robust carborate anions $[HexCB_{11}Cl_{11}]^-$ is described. $Mg[HexCB_{11}Cl_{11}]_2$ (**1**), prepared by reaction of $Mg(^nBu)_2$ with 2 equiv of $[Ph_3C][HexCB_{11}Cl_{11}]$, consists, in the solid state, of a central Mg^{2+} surrounded by two $[HexCB_{11}Cl_{11}]^-$ anions. In solution, experimental and classical molecular dynamics simulations (cMD) agree with cation/anion association being retained, reflecting the high electrophilicity of the Mg center. Yet, reflecting only weak anion/cation interactions, species **1** polymerizes 1-hexene and coordinates alkynes. However, **1** displays no reaction with $HSiEt_3$ at room temperature, consistent with a low hydridicity of the hard (HSAB) Mg^{2+} center. Contrasting with **1** (FIA = 264 kJ mol^{-1}; FIA: Fluoride Ion Affinity), salt $Mg[(nBu)_3NB_{12}H_4Cl_7]_2$ (**2**), incorporating the more basic ammoniododecaborate $[(nBu)_3NB_{12}H_4Cl_7]^-$ anion, is significantly less Lewis acidic (FIA = 214.7 kJ mol^{-1}) and unreactive with alkenes and alkynes. Salt **1** effectively catalyzes alkene/alkyne hydrosilylation via an initial alkene/alkyne coordination/initiation, as suggested by experimental and computational data. It also efficiently catalyzes (with a catalyst loading down to 0.1 mol%) the hydrosilylation of CO_2 to CH_4 in the presence of $HSiEt_3$. Salt **1** smoothly promotes the catalytic transfer hydrogenation of 1,1-diphenylethylene, and it is also an active imine hydrogenation catalyst in the presence of H_2.

Introduction

Strong Lewis acids and electrophilic species are of crucial importance for the mediation of numerous stoichiometric and catalytic transformations.[1–5] In this area, well-defined ligand-supported Mg^{II} species are gaining importance for use in catalysis due to the potent electrophilicity of the Mg^{II} center, favoring the activation of various substrates, with earth abundance, low toxicity, and low cost being additional attractive features of magnesium.[6] Neutral Mg^{II} species have mostly been shown to catalyze the heteroelementation of various polar/unsaturated substrates, with representative examples ranging from the hydro-silylation/-boration of alkenes/alkynes, nitriles, and carbonyl substrates (such as ketones, esters, and CO_2) to dehydrocoupling catalysis.[7–11] Notably, a couple of examples of Mg-catalyzed imine hydrogenation catalysis were also recently reported.[12,13] Though less explored than their neutral analogues, discrete cationic Mg^{II} complexes are of particular interest because the cationic charge at the Mg^{II} center enhances metal electrophilicity and thus substrate activation. Representative examples of ligand-supported Mg cations for use in catalysis include their application in cyclic esters ring-opening polymerization,[14,15] CO_2 hydro-silylation/-boration,[8,16] carbonyl hydroboration.[17] Noticeably, combining a cationic charge and low coordination at Mg^{II}, as in two-coordinate cations of the type $[(BDI)Mg]^+$ (BDI = β-diketiminate-type bidentate ligand), recently reported by Harder,[18,19] results in a highly electrophilic Mg center able to form isolable adducts with internal alkynes and various arenes, and catalyze alkyne hydrophosphination.[20]

Stabilization of Mg^{II} organocations by various *N*-/*O*-based ligand platforms as well as NHC ligands, has thus led to stable and soluble electrophilic entities enabling substantial substrate activation. However, ideally, maximal electrophilicity at Mg^{II} could be achieved with a simple "ligand-free" Mg^{2+} dication, though such a "naked" dication does not exist in the condensed phase. Toward this goal, Mg^{2+} dication stabilized only by properly designed weakly coordinating anions (WCAs), i.e., as $Mg[WCA]_2$ salts, may lead to soluble and stable sources of "pseudo-naked"/weakly coordinated Mg^{2+} dication. Thus far, such Mg salts are unknown and, more

[*] X. Xu, S. Tongdee, S. Munshi, B. Jacques, S. Dagorne
Institute of Chemistry, Université de Strasbourg, CNRS, Strasbourg 67000, France
E-mail: dagorne@unistra.fr
A. Chaumont, C. Gourlaouen
Laboratoire de Modélisation et Simulations Moléculaires, Université de Strasbourg, CNRS, Strasbourg 67000, France
R. Wehmschulte
Chemistry Program, Florida Institute of Technology, 150 West University Boulevard, Melbourne, FL 32901, USA
E-mail: rwehmsch@fit.edu

Additional supporting information can be found online in the Supporting Information section

generally, there are only rare examples of divalent metal salts M[WCA]$_2$ exhibiting stability and solubility in organic media, including: i) a Zn[WCA]$_2$ salt consisting of a central Zn^{2+} dication only weakly stabilized by two $[HexCB_{11}Cl_{11}]^-$ carborate anions,[21] ii) the Sr[Al{OC(CF$_3$)$_3$}$_4$]$_2$ salt featuring a rather large Sr^{2+} dication partially associated with the alanate anions,[22] and iii) a very recent Ca[Al{OC(CF$_3$)$_3$}$_4$]$_2$ salt, though not structurally authenticated and only stable in SO_2 solution.[23] Taking the example of salt Zn[HexCB$_{11}$Cl$_{11}$]$_2$, it is the strongest Zn-based Lewis acid in solution, validating the approach of associating a divalent M^{2+} center with halogenated carborates as WCAs for unprecedented electrophilicity. We now report on the synthesis and structural characterization of the first Mg[WCA]$_2$ salt, incorporating a central Mg^{2+} stabilized by two $[HexCB_{11}Cl_{11}]^-$ carborate anions. The stability and solubility of Mg[HexCB$_{11}$Cl$_{11}$]$_2$ also allowed reactivity studies with various polar/unsaturated substrates, all in line with a highly electrophilic Mg^{II} center. Further, classical molecular dynamic simulations combined with DFT calculations provided critical insights into its solution structure and mechanistic aspects, rationalizing the observed reactivity.

Results and Discussion

Synthesis and Structure

To access Mg[WCA]$_2$ salts as potential sources of "pseudo-free" or weakly stabilizing Mg^{2+} dication, the use of the classical $[B(C_6F_5)_4]^-$ borate anion as a possible counterion was initially studied through an attempted synthesis of Mg[B(C$_6$F$_5$)$_4$]$_2$. To this end, Mg(^{n}Bu)$_2$ was reacted with 2 equiv of [Ph$_3$C][B(C$_6$F$_5$)$_4$] (C$_6$D$_5$Br, 1 h, RT; eq. 1): both reagents are quantitatively consumed affording an intractable mixture of [Mg-C$_6$F$_5$]-incorporating species according to ^{1}H and ^{19}F NMR data, consistent with anion degradation and indicating that a more chemically robust anion is required.[24] Next, the much more robust $[Al\{OC(CF_3)_3\}_4]^-$ anion, popularized by Krossing, was investigated as a possible WCA.[25] The reaction of Mg(^{n}Bu)$_2$ with 2 equiv [Ph$_3$C][Al{OC(CF$_3$)$_3$}$_4$][26] (PhBr or 1,2-difluorobenzene, 1 h, RT; eq. 2) led to the formation of Mg[Al{OC(CF$_3$)$_3$}$_4$]$_2$ as the major product, according to ^{1}H, ^{19}F and ^{27}Al NMR data, along with unidentified side species (see Supporting Information). Yet, in our hands, isolation of pure Mg[Al{OC(CF$_3$)$_3$}$_4$]$_2$ could not be achieved from the crude mixture despite several attempts, precluding further studies.

$$\begin{array}{c} Mg(^nBu)_2 \\ + \\ 2[Ph_3C][B(C_6F_5)_4] \end{array} \xrightarrow[\begin{array}{c}-Ph_3CH\\-butene\end{array}]{RT,1h,PhBr} \textit{mixture of } Mg-C_6F_5 \textit{ species} \qquad (1)$$

$$\begin{array}{c} Mg(^nBu)_2 \\ + \\ 2[Ph_3C][Al\{OC(CF_3)_3\}_4] \end{array} \xrightarrow[\begin{array}{c}-Ph_3CH\\-butene\end{array}]{RT,1h,DFB} \begin{array}{c} Mg[Al\{OC(CF_3)_3\}_4]_2 \\ crude \\ not\ isolated \end{array} \qquad (2)$$

$$\begin{array}{c} Mg(^nBu)2 \\ + \\ 2[Ph_3C][HexCB_{11}Cl_{11}] \end{array} \xrightarrow[\begin{array}{c}-Ph_3CH\\-butene\end{array}]{RT,1h,DFB} \begin{array}{c} Mg[HexCB_{11}Cl_{11}]2 \\ 1 \end{array} \qquad (3)$$

Equations 1–3. Synthesis attempts of Mg[WCA]$_2$ and synthesis of Mg[HexCB$_{11}$Cl$_{11}$]$_2$ (**1**).

Fortunately, the chemically robust carborate anion $[HexCB_{11}Cl_{11}]^-$ proved suitable to access pure Mg[WCA]$_2$ species.[24,27] Thus, the double ionization reaction of Mg(^{n}Bu)$_2$ with 2 equiv [Ph$_3$C][HexCB$_{11}$Cl$_{11}$], prepared according to a literature procedure,[21] proceeds smoothly (DFB, 1 h, RT) to quantitatively produce salt Mg[HexCB$_{11}$Cl$_{11}$]$_2$ (**1**, eq. 3) along with Ph$_3$CH and polybutene (due to polymerization of the generated 1-butene). Salt **1** was isolated in 80% yield as an off-white solid. It is soluble and stable for days at room temperature in aromatic solvents such as PhBr and DFB, while decomposing within minutes to unknown species in dichloromethane. Alternatively, a salt metathesis reaction between MgI_2 and 2 equiv of Ag[HexCB$_{11}$Cl$_{11}$] (MeOH, RT) was also attempted to prepare salt **1**. Though the reaction proceeded as expected to afford a MeOH-stabilized Mg^{2+} dication associated with two non-coordinated $[HexCB_{11}Cl_{11}]^-$ anions, crude **1** could not be further purified (see Supporting Information for additional details).

The molecular structure of the Mg salt **1**, depicted in Figure 1, was established through X-ray diffraction studies. It consists of a central Mg^{2+} dication in an octahedral environment due to the association of the two $[HexCB_{11}Cl_{11}]^-$ anions in a κ^3-Cl_3 coordination mode. The Mg–Cl distances in **1** (2.534(1) Å average) are longer than those in the neutral complex [(THF)$_4$MgCl$_2$] (2.45 Å average)[28] and the dinuclear Mg cation [(THF)$_3$Mg(μ-Cl)$_3$Mg(THF)$_3$]$^+$ (2.507 Å average).[29,30] Due to the coordination to Mg^{2+}, the B–Cl bond distances of the Mg-coordinated chlorines (1.810 Å average) are lengthened relative to those in free $[HexCB_{11}Cl_{11}]^-$ (1.76 Å average). A similar lengthening of the involved B–Cl bonds also occurs upon association of $[HexCB_{11}Cl_{11}]^-$ with Zn^{II} mono- and di-cations.[21,31] As anticipated, the interactions between the central Mg^{2+} center and the surrounding chlorine atoms are purely electrostatic, as indicated by DFT-estimated non-covalent interactions (NCI, Figure 2).

In solution (C$_6$D$_5$Br, RT), ^{11}B NMR data of salt **1** agree with an effective coordination of the two $[HexCB_{11}Cl_{11}]^-$ anions to the Mg^{2+} dicationic center, with the presence of two resonances (δ −5.3 and −10.8 ppm), contrasting with the ^{11}B NMR spectrum for unassociated/"free" $[HexCB_{11}Cl_{11}]^-$ anion (as in [Ph$_3$C][HexCB$_{11}$Cl$_{11}$])[21] containing three distinct signals (δ −2.9, −10.0 and −11.6 ppm) under identical conditions. Similar NMR data were obtained in DFB, a more polar solvent, also suggesting $[HexCB_{11}Cl_{11}]^-$ coordination to Mg^{2+}. On the other hand, DOSY NMR measurements for a C$_6$D$_5$Br solution of **1** (RT) led to an estimated hydrodynamic volume of 1160 Å^3 (see Supporting Information). The latter value lies between the volume of salt **1** from solid state data (approximated to

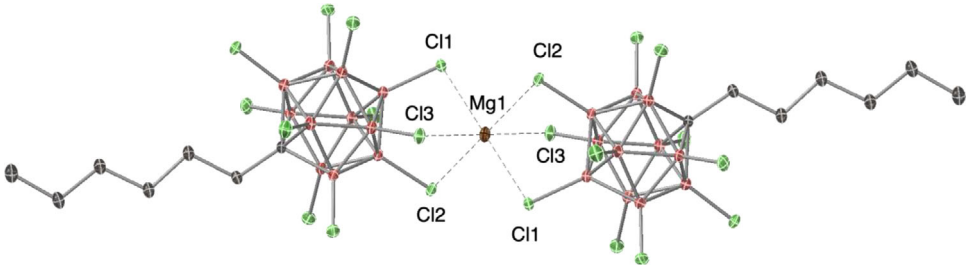

Figure 1. Molecular structure of $Mg[HexCB_{11}Cl_{11}]_2$ (**1**) with partial atom labeling for clarity. Selected bond distances (Å): Mg1–Cl1 = 2.5031(3), Mg1–Cl2 = 2.5276(2), Mg1–Cl3 = 2.5712(3), B1–Cl1 = 1.812(1), B2-Cl2 = 1.809(1), B3–Cl3 = 1.811(1).

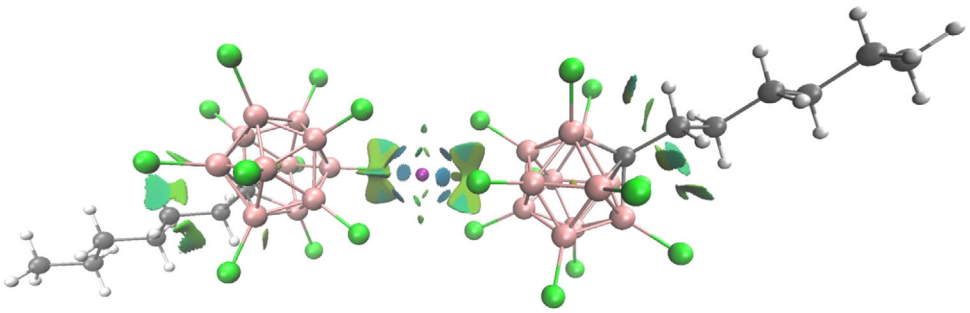

Figure 2. Non-covalent interactions (NCI) for a model species salt **1** as estimated by DFT (B3LYP/6–31 + G**). The central Mg^{2+} dication is in purple and the surrounding chlorine atoms are in green. Attractive electrostatic and dispersive interactions appear in blue and green.

1460 Å^3 following a known methodology)[32] and that of the carborate anion $[HexCB_{11}Cl_{11}]^-$ (720 Å), which could be consistent with salt **1** undergoing a fast cation/anion dissociation on the NMR timescale under the studied conditions. Yet, given the presence of two hexyl chains in **1** (at both ends), which are fluxional groups in solution, the hydrodynamic volume of **1** may significantly differ from that in the solid state, limiting the accuracy/validity of such a comparison.

To gain further insight on the solution structure of the Mg salt **1**, classical molecular dynamics (cMD) simulations were performed by modeling the structure/fluxional behavior of a model of **1** (**I**) within a solvent (PhBr) box (size of 70 x 70 x 70 Å, including roughly 1000 molecules of PhBr) using the Amber 18.0 software (see Supporting Information for further details). The trajectory consisted of a simulation of 2 µs at T = 298.15 K during which the system was let to evolve. A cumulative view of the trajectory is shown in Figure 3, where all snapshots of the structure of **I** (taken every 10 ns along the trajectory) are superposed, while the trajectory may be visualized (see video, Supporting Information). These data clearly indicate that both $[HexCB_{11}Cl_{11}]^-$ anions essentially remain κ^3-Cl_3 coordinated to the Mg^{2+} center, with Mg-Cl distances (2.47(1) Å average) similar to those observed in the solid state for **1** (2.533(1) Å average). Importantly, the cMD-estimated diffusion coefficient of **I** under the simulation conditions ($D = 2.5 \pm 0.7\ 10^{-10}$ m^2 s^{-1} at T = 298.15 K) matches well that experimentally estimated from DOSY NMR data for **1** in C_6D_5Br ($D = 2.94 \pm 0.58\ 10^{-10}$ m^2 s^{-1} at T = 298 K), providing experimental support to the proposed

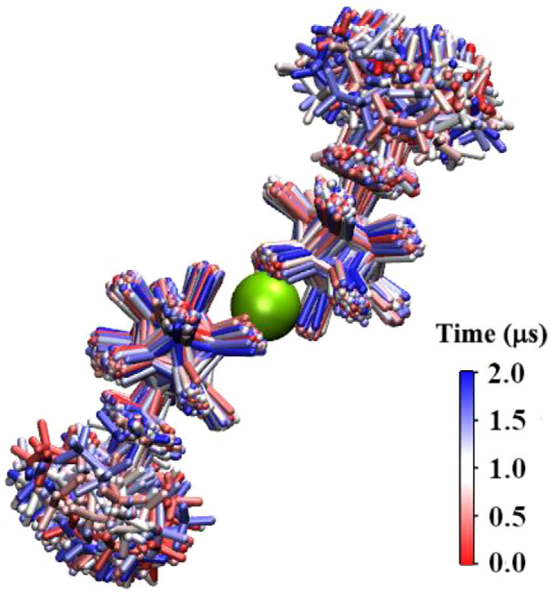

Figure 3. Cumulative view of the structures of modeled salt **1** (model **I**) in PhBr (70 × 70 × 70 Å^3 box) along the cMD simulation. The central Mg^{2+} dication is in green. A snapshot was taken every 10 ns along the 2 µs-long simulated trajectory. The color of the $[HexCB_{11}Cl_{11}]^-$ anions evolves as a function of the simulation time according to the color bar represented at the bottom right.

cMD approach. Therefore, as observed in the solid state, salt **1** likely consists of associated Mg^{2+} and $[HexCB_{11}Cl_{11}]^-$ ions in PhBr at RT, reflecting the strong Lewis acidity of the Mg^{2+}

center. Similarly, salt **1** does not presumably dissociate in DFB, given the similar NMR data for **1** in both solvents.

For comparison to the Mg carborate species **1**, salt $Mg[(nBu)_3NB_{12}H_4Cl_7]_2$ (**2**), incorporating the more coordinating/Lewis basic ammonio-dodecaborate $[(nBu)_3NB_{12}H_4Cl_7]^-$ anion, was also targeted and prepared following an aqueous route previously established for the synthesis of the Zn analogues.[33] The reaction of $MgCl_2{\cdot}H_2O$ with 2 equiv of the acid $[H(H_2O)_n][(nBu)_3NB_{12}H_4Cl_7]$, prepared by following a literature procedure,[33] led to the formation of salt **2** according to all characterization data (see Supporting Information for more details). The molecular structure of the Mg salt **2**, as established through X-ray diffraction studies (Figure S23, Supporting Information), features a central Mg^{2+} di-cation in a similar octahedral environment to that observed for the carborate salt **1**, with the κ^3-*Cl*$_3$ coordination of the two $[(nBu)_3NB_{12}H_4Cl_7]^-$ anions to Mg^{2+}. The Mg–Cl distances in **2** (2.513(2) Å average) are close, though a bit shorter, to those in **1** (2.533(1) Å average). In solution at RT, ^{1}H and ^{11}B NMR data agree with salt **2** retaining its solid-state structure in both C_6D_5Br and DFB.

Lewis Acidity Estimation

To assess the Lewis acidity of salts **1** and **2**, their fluoride ion affinity was evaluated by DFT (B3LYP/6–31 + G**, PhBr, see Supporting Information).[34,35] Consistent with a highly electrophilic Mg^{II} center, the FIA value for salt **1** (264 kJ mol^{-1}) is significantly higher than that of $B(C_6F_5)_3$ (220.5 kJ mol^{-1}), reflecting the strong Lewis acidity of **1**. Despite Mg^{2+} being a harder Lewis acid than Zn^{2+} (HSAB theory), the FIA of **1** is similar to that of its Zn analogue $Zn[HexCB_{11}Cl_{11}]_2$ (262.1 kJ mol^{-1}), which is probably due to a stronger anion/cation association of the Mg salt **1**. In contrast, the FIA of the ammonio-dodecaborate Mg salt **2** (214.7 kJ mol^{-1}) is in line with a significantly less electrophilic Mg^{II} due to stronger coordination of the $[(nBu)_3NB_{12}H_4Cl_7]^-$ anions to the metal center.

To probe the potential super Lewis acidic character of salt **1**,[36] its reactivity with the anion $[SbF_6]^-$ was studied. Salt **1** immediately and quantitatively reacts with 2 equiv of $[(nBu)_4N][SbF_6]$ (DFB, RT, 15 min) via a $[HexCB_{11}Cl_{11}]^-/[SbF_6]^-$ anion exchange to afford $Mg[SbF_6]_2$ and non-coordinated carborate anions, as deduced from ^{1}H and ^{11}B NMR data. Remarkably, the resulting mixture is stable under the studied conditions with no observable change after 24 h at RT, suggesting that $Mg[SbF_6]_2$ is a viable and stable salt in DFB solution and that salt **1** is not super Lewis acidic in DFB. In contrast, performing the same reaction in a 4/1 DFB/C_6D_5Br solvent mixture led after 2 h at room temperature to the formation of a mixture of fluorinated aromatics resulting from C_6D_5Br fluorination along with $[SbF_6]^-$ decomposition, according to NMR characterization including ^{1}H, ^{2}H, ^{19}F, ^{11}B, and 2D NMR data (see Supporting Information for additional details). Though the formation of a strong fluorinating agent is obvious, the formation of insoluble and not identified solids (possibly of type [Mg-F] and related aggregates) as the reaction proceeded prevented any further characterization and thus any clear-cut conclusion. However, in line with the behavior of salt **1** in DFB, the DFT-estimated FIA of SbF_5 (337.5 kJ mol^{-1}, PhBr) lies well-above that of salt **1** (264 kJ mol^{-1}, PhBr) suggesting that salt **1** is not a super Lewis acid.

Reactivity with Alkenes and Alkynes

Given its electrophilic nature, the reactivity of salt **1** was first probed for activation of unsaturated substrates such as alkenes and alkynes. As an initial test, the reaction of salt **1** with 1 equiv of 1-hexene (C_6D_5Br or DFB, 5 min) led to the immediate formation of polyhexene. Further indicative of a highly Lewis acidic Mg^{II} center in **1**, it quantitatively polymerized 100 equiv of 1-hexene within 20 min (C_6D_5Br, RT) to produce ill-defined polyhexene according to ^{1}H NMR and GPC data (see Supporting Information) with salt **1** retaining its integrity; a reaction probably proceeding through a Lewis acid-assisted cationic polymerization. For comparison, salt **1** is more reactive than its Zn analogue toward 1-hexene, which under identical conditions, converted 60% of 1-hexene to polymer after 3 h at RT. No reaction between the less Lewis acidic Mg salt **2** and 1-hexene (100 equiv) was observed after 24 h (C_6D_5Br, RT). Contrasting with its reactivity toward 1-hexene, salt **1** showed no apparent reaction with cyclohexene (1 or 4 equiv, DFB) after 16 h at room temperature, though polymerization to polycyclohexene occurs at 80 °C (complete cyclohexene conversion within 1 h of a 1/4 **1**/cyclohexene mixture). From a 1/4 **1**/cyclohexene mixture, no evidence of cyclohexene coordination to the Mg cationic center could be detected by low-temperature ^{1}H and ^{11}B NMR analysis (DFB, −30 °C). To promote alkene coordination to **1,** possibly through chelate formation, the *bis*-alkene 1,5-cyclooctadiene (1,5-COD) substrate was thus studied next, with no observable reaction at room temperature of a 1/2 **1**/1,5-COD solution in DFB from NMR data. However, low temperature ^{11}B NMR data (DFB, −30 °C) of the mixture indicated a splitting of the major ^{11}B NMR resonance (δ −10.7 ppm for salt **1**, DFB, −30 °C) to two resonances (δ −9.9 and −10.5 ppm), in line with a weaker cation/anion association upon addition of 1,5-COD. For comparison, the non-coordinated/"free" $[HexCB_{11}Cl_{11}]^-$ anion also features two such resonances but with a larger chemical shift difference (δ −9.9 and −11.8 ppm; see Figures S44 and S45). These data suggest a labile association/coordination of 1,5-COD to the Mg center under the studied conditions.

The reaction of salt **1** with alkynes such as 1-octyne, 2-hexyne, and 2,6-octadiyne was also evaluated for coordination to the Mg center. The ^{11}B NMR spectrum of a 1/6 **1**/1-octyne mixture (DFB, RT, 5 min) displays a significant broadening of the anion ^{11}B NMR signals, indicative of a lower cation/anion association, suggesting 1-octyne coordination to the Mg^{2+} center. Similarly, the reaction of **1** with 1 equiv of 2-hexyne provoked an immediate broadening of the ^{11}B NMR major peak (see Supporting Information). In addition, low temperature ^{1}H and ^{11}B NMR data of a 1/4 **1**/2-hexyne mixture (DFB, −30 °C) agree with the formation of labile alkyne···Mg adducts under the studied conditions, with the ^{11}B

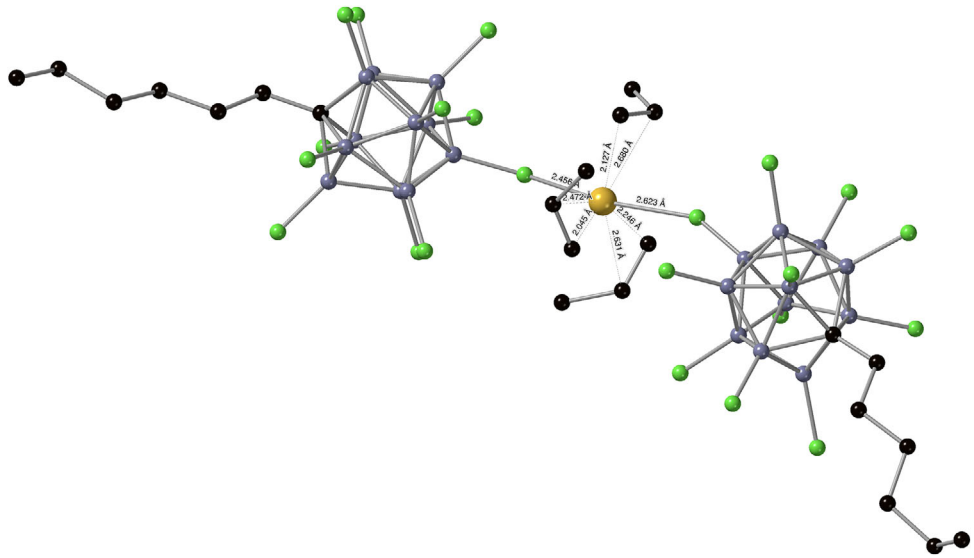

Figure 4. Molecular structure of model $[Mg(propene)_3][HexCB_{11}Cl_{11}]_2$ as calculated from the cMD trajectory (7.5 μs long) for a mixture of **I** and 100 propene molecules in PhBr (70 × 70 × 70 Å^3 box). Snapshot taken along the trajectory at t = 7051 ns. Labels are omitted for clarity. The central Mg^{2+} dication is in yellow and the surrounding carbon and chlorine atoms are in black and green, respectively.

NMR signals in line with a lower cation/anion association as well as downfield shifted 2-hexyne resonances ($\Delta\delta = 0.06$ ppm average vs. free 2-hexyne; see Figures S50 and S51). To further promote/stabilize alkyne coordination, *bis*-alkyne 2,6-octadiyne was reacted with salt **1**. The reaction of salt **1** with 2 equiv 2,6-octadiyne (DFB, RT, 15 min) led to an immediate broadening of the ^{11}B NMR resonances, suggesting a dynamic process. At −30 °C (Figures S52 and S53), the ^{11}B NMR spectrum is similar to that of a free or weakly interacting $[HexCB_{11}Cl_{11}]^-$ anion, clearly indicating alkyne coordination to the Mg^{2+} dication. Although the formation of a [*bis*(*bis*-alkyne)Mg]$^{2+}$ dication seems possible, the rather broad ^{1}H NMR signals suggest labile coordination/chelation even under the studied conditions. To date, characterized alkyne-Mg cationic adducts are rare, and only mono-alkyne adducts are known as described by Harder and coworkers by coordination to a [(BDI)Mg]$^+$ cation (BDI = β-diketiminate).[19] In the present case, despite their apparent stability over time (24 h, RT, PhBr or DFB), such cationic adducts could not be isolated and further characterized, possibly due to their labile nature.

To gain additional insight/support on alkene and alkyne reactivity with salt **1**, DFT and cMD calculations were performed. Taking propene as model, the DFT-computed Gibbs free energy for the reaction of **I**, model of salt **1**, with a propene molecule to afford adduct $[(HexCB_{11}Cl_{11})Mg(propene)]^+$ along with a fully dissociated $[HexCB_{11}Cl_{11}]^-$ anion is quite endergonic ($\Delta G = 61.5$ kJ mol^{-1}, PhBr), inconsistent with the observed fast reaction of **1** with 1-hexene.

On the other hand, cMD simulations gave a better understanding of salt **1** dynamic behavior and reactivity in PhBr solution. cMD simulation of **I** (PhBr box, 7.5 μs long simulation, RT) in the presence of 100 propene molecules indicates the ready coordination of propene to the Mg center with the formation of *bis*- and *tris*-propene cationic adducts as major species (Figure 4; Figure S68 and video in the ESI). Importantly, as deduced from potential mean force (PMF) calculations (Table S7, ESI), the coordination of one propene to the Mg cationic center of **I** is thermodynamically feasible under the studied conditions ($\Delta G = 2.1$ kJ mol^{-1}) and proceeds with a low energy barrier (26.4 kJ mol^{-1}), consistent with a fast and labile alkene coordination to the Mg center. Considering all *tris*-propene Mg adducts $[Mg(\eta^2\text{-propene})_3][HexCB_{11}Cl_{11}]_2$ computed along the cMD trajectory, they consist of three dissymmetrically Mg-bound propene ligands with $Mg–C1_{propene}$ distances (2.12(1) Å average) significantly shorter than the $Mg–C2_{propene}$ (2.68(1) Å average), with a representative example of such $[Mg(\eta^2\text{-propene})_3][HexCB_{11}Cl_{11}]_2$ adduct being depicted in Figure 4. The calculated (average) $Mg–C1_{propene}$ distances in *tris*-propene adducts are similar to the Mg–alkyl σ-bond length,[37] supporting substantial alkene activation upon coordination to the Mg^{II} center, and thus susceptible to undergo cationic polymerization as observed with 1-hexene in the presence of **1**. For comparison, a dissymmetrical alkene bonding/contact to Mg^{II} was also observed in a structurally characterized neutral $Mg(\eta^2\text{-alkene})_2$ dibenzoazepinate complex, albeit with longer and less dissymmetrical Mg–C contacts (2.740(3) and 2.848(3) Å average for the shorter and longer distances, respectively).[38] Apart from propene activation by the Mg^{2+} cation, it is also noteworthy that the two $[HexCB_{11}Cl_{11}]^-$ anions essentially remain η^1-coordinated, each through a chlorine atom, to the Mg^{II} center (Mg···Cl distance = 2.69(1) Å average), thus readily adapting their coordination mode (from κ^3-Cl_3 to η^1-Cl) in solution upon incoming alkene substrates.

Similarly, cMD calculations of model **I** in the presence of 100 propyne molecules (in a PhBr box) also suggest the fast and labile coordination of propyne to the Mg^{II} center at room temperature, with the fast formation of *bis*-, *tris*-, and

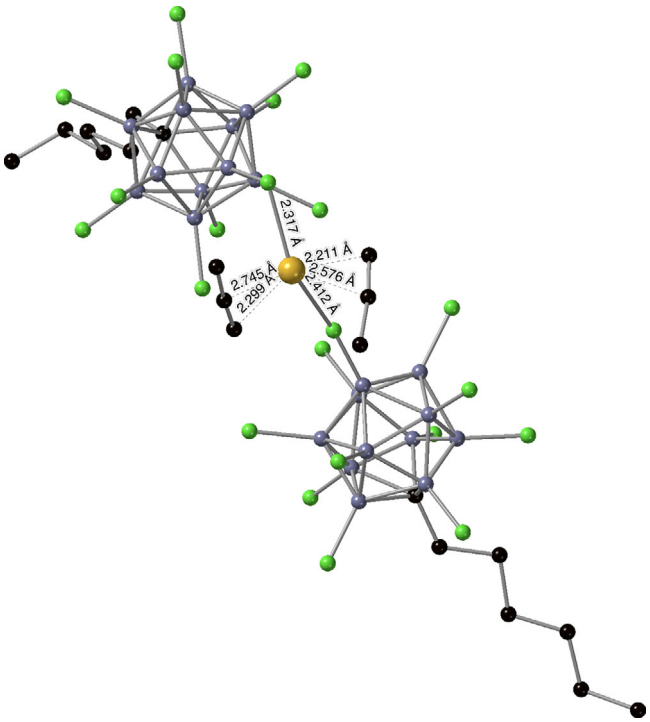

Figure 5. Molecular structure of a representative $[Mg(propyne)_2][HexCB_{11}Cl_{11}]_2$ model as calculated from the cMD trajectory (2 µs long) for a mixture of **I** and 100 propyne molecules in PhBr (70×70×70 Å^3 box). Snapshot taken along the trajectory at t = 354 ns. Labels are omitted for clarity. The central Mg^{2+} dication is in yellow, and the surrounding carbon and chlorine atoms are in black and green, respectively.

tetra-propyne Mg^{II} adducts that readily interconvert through fast propyne coordination/decoordination (see Supporting Information for a video and Figure 5 for a representative cMD-computed *bis*-propyne Mg adduct). This is further confirmed by PMF calculations indicating that coordination of a propyne molecule to **I** is slightly exergonic ($\Delta G = -1.3$ kJ mol^{-1}) with a low energy barrier (16.8 kJ mol^{-1}), in line with a labile propyne coordination. In the modeled *bis*-propyne adducts, the alkyne molecules also coordinate dissymmetrically to Mg^{2+} with $Mg\cdots C1_{propyne}$ distances (2.26(1) Å average) shorter than $Mg–C2_{propyne}$ distances (2.67(1) Å average). The Mg–alkyne contact/bond lengths in such adducts are comparable to those in a mono-cationic alkyne adduct, $[(BDI)Mg(2\text{-butyne})]^+$, recently characterized.[19]

Reactivity with $HSiEt_3$

The activation of the Si–H bond is well-established for a number of strong Lewis acids, most notably for $B(C_6F_5)_3$ and $Al(C_6F_5)_3$,[39–41] and is typically considered as the key initial step for Lewis-acid-mediated hydrosilylation of various unsaturated substrates. Probing the reactivity of Lewis acidic salt **1** with $HSiEt_3$ as an Si–H source (1/100 **1**/$HSiEt_3$ mixture, C_6D_5Br, RT) led to no apparent reaction after 24 h according to ^1H and $^{29}Si\{^1H\}$ NMR data, contrasting with the rather

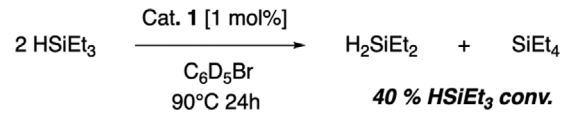

Scheme 1. Reaction of the Mg salt **1** with $HSiEt_3$.

fast $HSiEt_3$ redistribution observed with the Zn counterpart $Zn[HexCB_{11}Cl_{11}]_2$ under identical conditions.[21] Consistent with the latter, the DFT-estimated hydride ion affinity (HIA, PhBr) of salt **1** (HIA = 370 kJ mol^{-1}) is significantly lower than that of $Zn[HexCB_{11}Cl_{11}]_2$ (HIA = 496 kJ mol^{-1}), clearly indicating that salt **1** is a harder Lewis acid than its Zn analogue.[36] Nevertheless, heating a 1/100 **1**/$HSiEt_3$ mixture (C_6D_5Br) at 90 °C promoted silane redistribution with a 40% $HSiEt_3$ conversion to 1/1 $H_2SiEt_2/SiEt_4$ mixture after 24 h as deduced from NMR data (Scheme 1).

As DFT-estimated, the reaction of model **I** (model of **1**) with one $HSiEt_3$ molecule to mono-cation $[(HexCB_{11}Cl_{11})Mg(HSiEt_3)]^+$ (and free $[HexCB_{11}Cl_{11}]^-$) is clearly endergonic ($\Delta G = 77.7$ kJ mol^{-1}). Likewise, the reaction of such $Mg\cdots HSiEt_3$ adduct with an additional $HSiEt_3$ to yield $[(HexCB_{11}Cl_{11})MgH]$ and $[Et_3Si–H–SiEt_3]^+$ is disfavored thermodynamically ($\Delta G = 69.7$ kJ mol^{-1}). Yet, upon forcing conditions, the formation of trace amounts $[Et_3Si–H–SiEt_3]^+$ seems possible, and would account for the observed $HSiEt_3$ redistribution reaction slowly proceeding at 90 °C.

cMD simulations of model **I** in the presence of 100 $HSiEt_3$ molecules (in a PhBr box) further indicate the low reactivity of $HSiEt_3$ with **1**. As illustrated in Figure 6, the calculations agree with little to no $Mg^{2+}/HSiEt_3$ interactions under simulation conditions (PhBr, RT) with most $HSiEt_3$ molecules being outer-sphere, as indicated by long $Si–H\cdots[Mg]^{2+}$ distances all above 3.5 Å (see also a video in the ESI). Accordingly, unlike propene and propyne, PMF-estimated $HSiEt_3$ coordination to the Mg center in **I** is quite endergonic (39.8 kJ mol^{-1}) while no energy barrier could be computed.

Alkene and Alkyne Hydrosilylation Catalysis

Mg-catalyzed alkene and alkyne hydrosilylation catalysis has thus far been little investigated, and essentially includes contributions from the groups of Parkin and Hill, showing that well-defined Mg–H species may mediate alkene/alkyne hydrosilylation catalysis through an insertion/σ-bond metathesis sequence, albeit with low catalytic activity.[8,42,43] Alternatively, in principle, Mg-mediated alkene/alkyne hydrosilylation should also be achievable through Lewis acid-promoted catalysis with a proper Mg-based Lewis acid such as salt **1**. Satisfyingly, the reaction of a 1/1 1-hexene/$HSiEt_3$ mixture with salt **1** as catalyst (1 mol% of **1**, C_6D_5Br) led to the immediate and quantitative formation of the *anti*-Markovnikov hydrosilylation product **3** within 10 min at room temperature (Scheme 2), with catalyst **1** retaining its integrity thus agreeing with a Lewis acid type mechanism. For comparison, 1-hexene hydrosilylation catalyzed by Mg–H complexes of the type $[(BDI)Mg–H]_2$

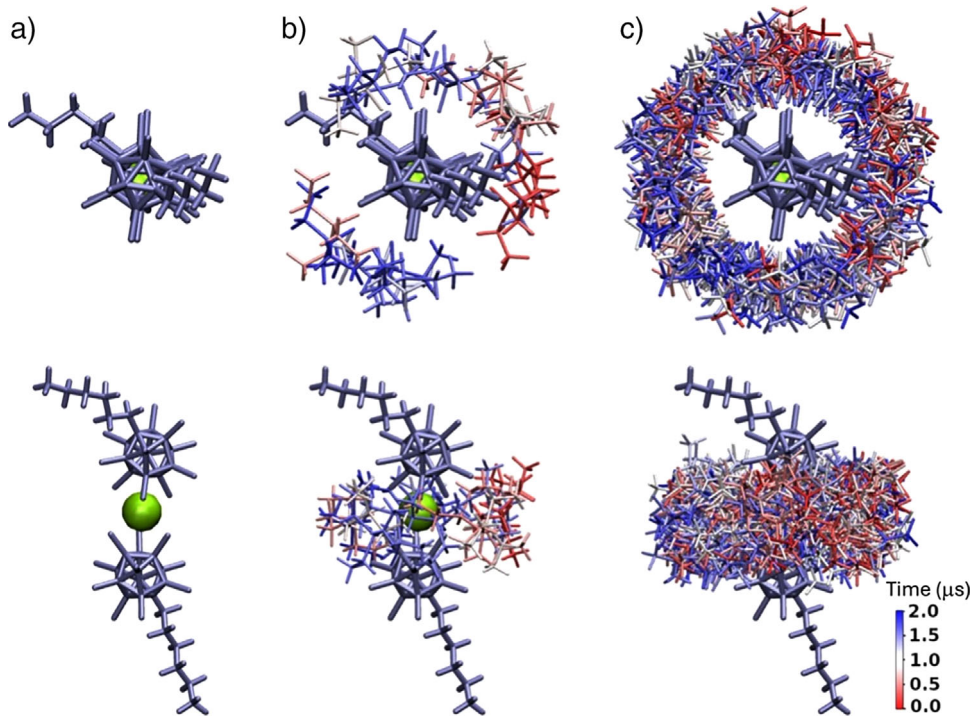

Figure 6. Cumulative view of $HSiEt_3$ molecules interactions with salt **I**, with distances between the Si-*H* hydrogen and the Mg^{2+} center within a) 3.5, b) 4.0, and c) 4.5 Å, as computed from a cMD simulation of model **I** in the presence of 100 $HSiEt_3$ modelled molecules ($70 \times 70 \times 70$ Å^3 box of PhBr molecules, 2 μs trajectory, room temperature.) $HSiEt_3$ are color-coded as a function of the time step of the trajectory. The corresponding color bar (in μs) is given in the bottom right corner. The central Mg^{2+} dication is in green.

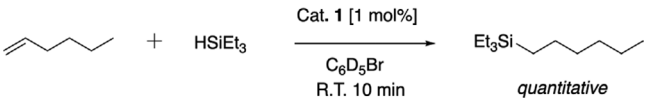

Scheme 2. 1-hexene hydrosilylation catalyzed by the Mg salt **1**.

(BDI = β-diketiminate) requires days for reaction completion at higher catalyst loading and reaction temperature.[42]

Likewise, the Mg salt **1** also effectively catalyzes alkyne hydrosilylation, with the reaction of a 1/1 1-octyne/$HSiEt_3$ mixture in the presence of **1** (1 mol%) affording hydrosilylation products **4**–**6** in a 3/1/1 **4**/**5**/**6** ratio (Scheme 3, 80% overall NMR yield) after 40 min at room temperature according to ^{1}H NMR and GC-MS data analysis. Given the experimental and *c*MD data on the relative reactivity of alkenes, alkynes and $HSiEt_3$ toward **1** (vide supra), the present hydrosilylation catalysis proceeds via an initial alkene/alkyne activation through coordination of the Mg^{II} center, rather than an initial Si–H activation as typically observed for most main group Lewis acid catalysts.[40,41,44] For instance and comparison, 1-hexene hydrosilylation catalyzed by $Zn[HexCB_{11}Cl_{11}]_2$ first involves $HSiEt_3$ ionization to form $[Et_3Si–H–SiEt_3]^+$ that then acts as the hydrosilylation catalyst.[21]

Additional mechanistic rationale and support were provided through cMD and DFT calculations (ωB97XD/6–31 + G**, PhBr as solvent through a PCM model; see Supporting Information for details) using modeled propene and propyne molecules for simplicity. Prior to DFT calculations and to obtain realistic starting models, cMD simulations were first conducted with a 100/100/1 propene (or propyne)/$HSiEt_3$/**I** mixture during a 2 μs trajectory (PhBr box, RT), from which representative models were extracted and used as starting points for DFT-computed mechanisms (for their molecular structures, see Figures S73, S78 and S82; ESI). As depicted in Figure 7 for propene hydrosilylation, cMD-estimated model **A**, consisting of a *tris*-propene Mg adduct (along with two carborate anions) in the vicinity of a $HSiEt_3$ molecule (Figure S73), may readily react through a Si–*H* hydride transfer to the C_β carbon of a Mg-coordinated propene moiety via transition state **TS1** (ΔG = 72.0 kJ mol^{-1}) to yield the rather high energy intermediate **B** (ΔG = 71.1 kJ mol^{-1}). The latter is only a fleeting intermediate since it consists of a newly formed Mg-propyl function that only weakly stabilizes a $[SiEt_3]^+$ cation through C_β–*H* interaction. It then reacts intramolecularly through a $[SiEt_3]^+$ electrophilic attack of the Mg-*propyl* group (**TS2**, ΔG = 107.5 kJ mol^{-1}) to afford hydrosilylation product **C** ($\Delta G = -36.0$ kJ mol^{-1}) and re-generate the Mg^{2+} dication.

Regarding propyne hydrosilylation, a one-step mechanism could be DFT-computed to account for the formation of the major product, **4** (Scheme 3), and is depicted in Figure 8. Thus, from the cMD-simulated model **D**, which incorporates a *bis*-propyne Mg adduct (along with two carborate anions) with an $HSiEt_3$ molecule in close proximity (Figure S78), the formation of the *anti*-hydrosilylation product may directly occur through a low-energy transition state **TS3** (ΔG = 46.4 kJ mol^{-1}) involving a Si–*H* transfer to a

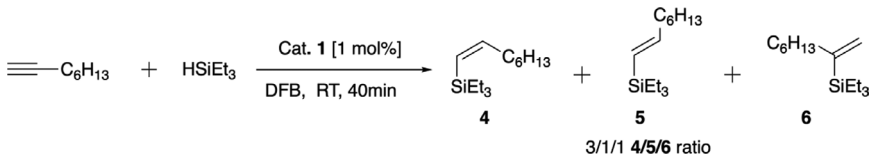

Scheme 3. 1-octyne hydrosilylation catalyzed by the Mg salt **1**.

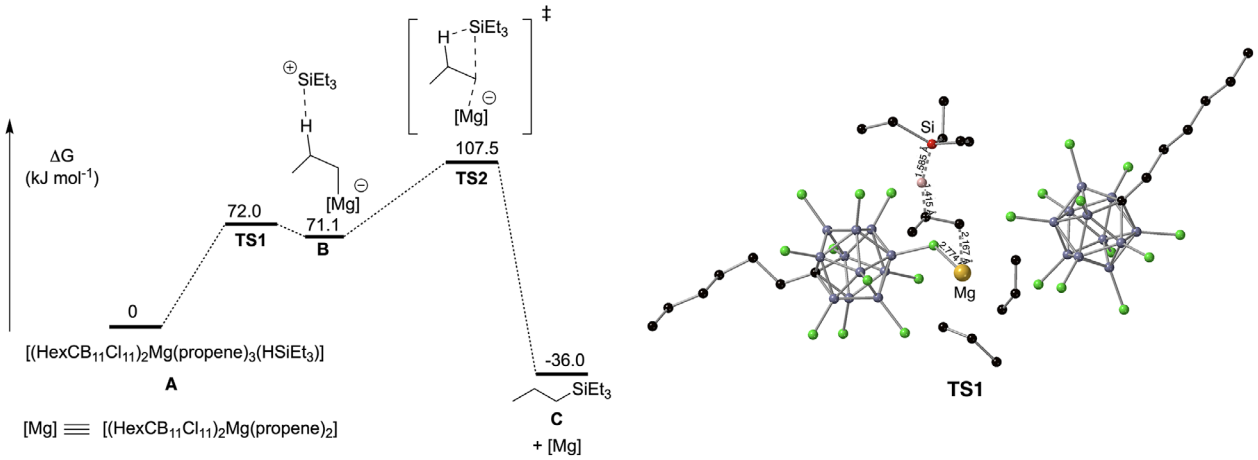

Figure 7. Left: DFT-estimated (ωB97XD/6–31 + G**) for the hydrosilylation of propene catalyzed by **I**, a model of Mg salt **1**. The molecular structure of the starting model **A** is depicted in Figure S73, as computed from *c*MD simulations. Right: molecular structure of **TS1** with the central Mg^{2+} dication in yellow while the surrounding carbon and chlorine atoms are in black and green, respectively.

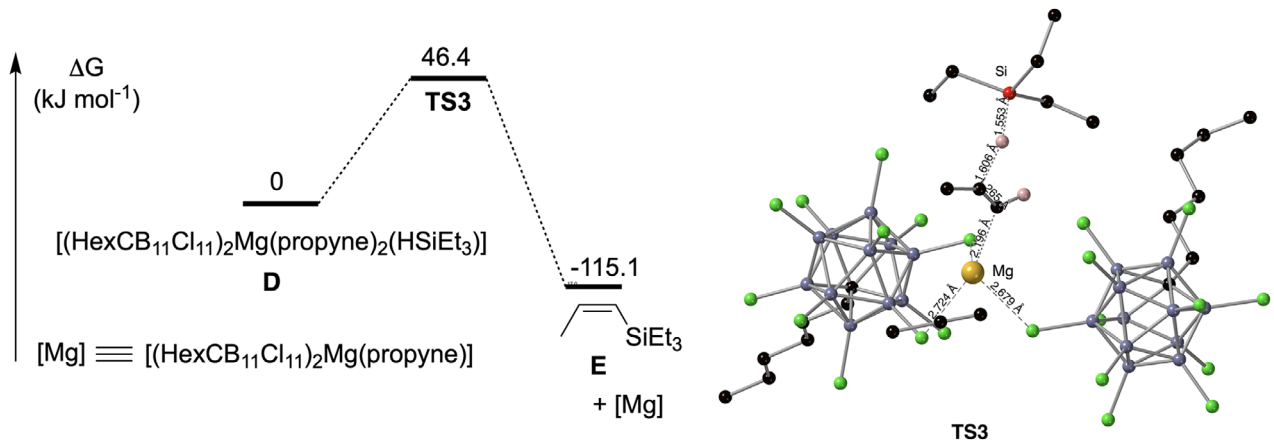

Figure 8. Left: DFT-estimated (ωB97XD/6–31 + G**) for the hydrosilylation of propyne catalyzed by model Mg salt **I** to form the major product **E**. The molecular structure of the starting model **D** is depicted in Figure S78, as computed from *c*MD simulations. Right: molecular structure of **TS3** with the central Mg^{2+} dication in yellow while the surrounding carbon and chlorine atoms are in black and green, respectively.

Mg-activated propyne (at C_β) having an apparent vinylic character (Figure 8, right). **TS3** then directly collapses to the exclusive formation of the *Z*-isomer hydrosilylation product (**E**, $\Delta G = -115.1$ kJ mol^{-1}).

Interestingly, the nature of the propyne Mg adduct undergoing hydrosilylation influences product selectivity according to calculations. Thus, computation of a propyne hydrosilylation pathway starting from a *c*MD-simulated model incorporating a *tetra*-propyne Mg adduct (Figure S82), which is significantly more hindered than the *bis*-propyne adduct analogue, led the formation of **E** as well as the α-isomer (Me)($SiEt_3$)C=CH_2 (model **H**, Figure S81), thus rationalizing the formation of minor product **6** in 1-octyne hydrosilylation catalyzed by **1**. The formation of the minor *E*-isomer (simplified model of **5**) could not be DFT-rationalized with a Mg-catalyzed process. However, trace amounts of $[SiEt_3]^+$ may form as the catalysis proceeds, which could account for the formation of **5**.[45] In this regard, an independent 1-octyne hydrosilylation catalysis run using in situ generated $[SiEt_3][HexCB_{11}Cl_{11}]$ as catalyst (1 mol%)

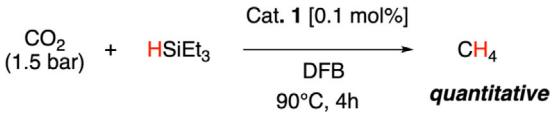

Scheme 4. CO_2 hydrosilylation catalyzed by Mg salt **1**.

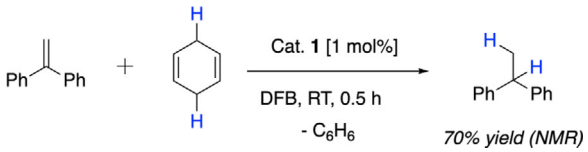

Scheme 5. Transfer hydrogenation catalysis mediated by salt **1**.

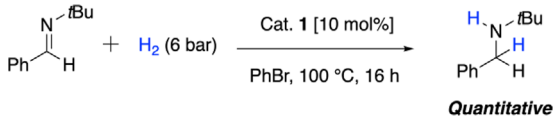

Scheme 6. Imine hydrogenation catalyzed by salt **1**.

led to a quantitative 1-octyne consumption within 20 min (C_6D_5Br, RT, ^1H NMR monitoring), with the predominant formation of polymeric material (not further characterized) along with 10%–15% formation of hydrosilylation products **4**, **5** and **6** in a roughly 1/1/1 ratio.

Carbonyl and CO_2 Hydrosilylation by Species 1

The potent Lewis acidity of Mg salt **1** also prompted its evaluation in carbonyl hydrosilylation catalysis, given the known activity of some strong Lewis acids, such as $B(C_6F_5)_3$ and various main group metal organocations,[40,46,47] for efficient hydrosilylation catalysis under mild conditions. Yet, no reaction was observed upon combining a 1/1 benzophenone/$HSiEt_3$ mixture with salt **1** (1mol) after 24 h at RT (and then 24 h at 90 °C), reflecting the strong oxophilicity/low hydridicity of the Mg^{II} center. ^1H and ^{11}B NMR monitoring of the mixture (C_6D_5Br) indicated the immediate formation of a benzophenone di-cationic adduct of the type $[Mg(O{=}CPh_2)_x]^{2+}$ (x = 4 to 6) along with free carborate anions. Under the studied conditions, benzophenone coordination apparently precludes any $Mg^{II}{\cdots}HSiEt_3$ interaction even upon heating, and thus silane activation that would permit/initiate catalysis.[40] An identical outcome was observed with benzaldehyde as a carbonyl source. In comparison, under identical conditions, the *softer* Lewis acid $Zn[HexCB_{11}Cl_{11}]_2$ is an efficient benzophenone hydrosilylation catalyst at room temperature (TOF up to 200 h^{-1}).[21]

In contrast, the Mg salt **1** was found to be more reactive with the less Lewis basic CO_2 under hydrosilylation conditions, though CO_2 is typically a more challenging C=O substrate to reduce.[48] Thus, species **1** (1 mol% vs. $HSiEt_3$) efficiently catalyzes CO_2 hydrosilylation (1.5 atm, CO_2, DFB, 90 °C) to the quantitative formation of methane along with siloxanes by-products, according to ^1H and ^{13}C NMR data. The present Mg-mediated CO_2 hydrosilylation catalysis,[8,16,49] is roughly twice as fast as that with $Zn[HexCB_{11}Cl_{11}]_2$ as catalyst and even proceeded effectively at lower catalyst loading (0.1 mol%) with complete $HSiEt_3$ conversion to methane in the presence of CO_2 (1.5 atm) within 4 h at 90 °C (Scheme 4). The present catalysis probably proceeds through a Lewis acid-type activation similar to Al- and Zn-based Lewis acidic catalysts.[46,50,51]

Hydrogenation Catalysis with Mg Salt 1

Catalytic hydrogenation of unsaturated substrates mediated by Mg^{II} metal complexes remains rare, and notably includes the use of Mg amido catalysts for imine hydrogenation catalysis[12] and Mg–H pincer complexes for the catalytic semi-hydrogenation of alkynes and alkene hydrogenation.[52] To probe the potential of Mg salt **1** for hydrogenation, transfer hydrogenation catalysis of 1,1-diphenylethylene was first tested using 1,4-cyclohexadiene (CHD) as the hydrogen source. Thus, salt **1** efficiently catalyzes such transformation with 80% conversion of 1,1′diphenylethylene to hydrogenation product Ph_2CH–Me (70% NMR yield, Scheme 5) along with a dimer of 1,1′-diphenylethylene (2,3-dihydro-1-methyl-1, 3,3-triphenyl-indene) as a minor product, within 30 min at room temperature.[53]

Species **1** was next evaluated for imine hydrogenation using molecular hydrogen. Though no reaction was observed at room temperature, salt **1** (10 mol%) satisfyingly catalyzes hydrogenation of (Ph)(H)C=N(*t*Bu) at 100 °C (PhBr) in the presence of H_2 (6 bar) with the quantitative formation of the corresponding amine product within 16 h (not optimized, Scheme 6). In contrast, salt **1** is inactive under hydrosilylation conditions, with no reaction between a 1/1 (Ph)(H)C=N(*t*Bu)/$HSiEt_3$ mixture and salt **1** (10 mol%) after 24 h at 100 °C (PhBr). The higher reactivity toward H_2 versus $HSiEt_3$ suggests a hydrogenation catalysis going through a FLP-type operative mechanism.[54,55] With **1**/(Ph)(H)C=N(*t*Bu) acting as the Lewis pair, an initial H_2 cleavage to a transient Mg–H of the type $[(HexCB_{11}Cl_{11})Mg{-}H][HexCB_{11}Cl_{11}]$ along with iminium $[(Ph)(H)C{=}NH(tBu)]^+$ likely occurs with a subsequent Mg–*H* transfer to produce the amine product and re-generate catalyst **1**.

Conclusion

Stable and soluble Mg^{2+} stabilized only by weakly coordinating $[HexCB_{11}Cl_{11}]^-$ carborate anions was shown to be accessible. All experimental and *c*MD data on salt **1** are consistent with anion coordination being retained in solution, reflecting the strong Lewis acidity of the central $[Mg]^{2+}$ dication. Nevertheless, in line with rather weak Mg···carborate interactions, unsaturated substrates such as alkene/alkynes readily coordinate the $[Mg]^{2+}$, with a terminal alkene like 1-hexene being immediately polymerized upon coordination. In contrast and reflecting to the low hydridicity of $[Mg]^{2+}$, salt **1** only exhibits low reactivity with hydrosilanes such as $HSiEt_3$. Overall, salt **1** stands as a strong Mg-based Lewis

acid and, as expected, is harder (HSAB) than $Zn[HexCB_{11}Cl_{11}]_2$.

Salt **1** was also exploited in hydrosilylation and hydrogenation catalysis. It is a highly effective catalyst for alkene/alkyne hydrosilylation under mild conditions, thus the first efficient Mg-based alkene/alkyne hydrosilylation catalyst. All data strongly suggest a catalyst proceeding through an alkene/alkyne coordination/initiation, rather than initial silane activation. In contrast, and again reflecting the hardness of the Mg^{2+}, salt **1** showed no hydrosilylation catalysis activity with imines and ketones, but it is effective in the catalytic hydrosilylation of CO_2, a less coordinative and Lewis basic substrate, with catalyst loading down to 0.1 mol%. Finally, salt **1** is also able to undergo FLP-type catalysis, as illustrated in the case of imine hydrogenation with molecular hydrogen.

From a methodological point of view, the present approach combining experimental characterization, *c*MD simulations, along with DFT calculations revealed crucial to understand the structure/reactivity trends of salt **1** in solution and should be useful for future developments and reactivity understanding of novel "pseudo-free" or weakly coordinated metal cations in the condensed phase.

Author Contributions

X.X., S.T., S.M.: experimental work. A.C.: cMD simulations and analysis. C.G.: DFT calculations and analysis. B.J.: supervision. R.W., S.D.: supervision, conceptualization, funding acquisition, data curation, formal analysis, writing—review & editing.

Supporting Information

NMR spectra, crystallographic details, DFT calculation details. CCDC 2431141 and CCDC 2431142 contain the supplementary crystallographic data for this paper. These data are provided free of charge by the joint Cambridge Crystallographic Data Centre and Fachinformationszentrum Karlsruhe (http://www.ccdc.cam.ac.uk/structures).

Acknowledgements

The University of Strasbourg and the CNRS are gratefully acknowledged for financial support as well as the Agence Nationale de la Recherche (ANR). S.M. thanks the ANR (project CarMaCat, ANR-22-CE07-0031-01) for a post-doctoral fellowship. X.X. thanks the Fondation Jean-Marie Lehn for a post-doctoral fellowship. For the X-ray crystallographic of salt **2**, the authors thank the National Science Foundation (grant CHE-1726630) and the University of Oklahoma (USA) for funds to purchase of the X-ray instrument and computers. This structure of **2** was determined by Douglas R. Powell.

Conflict of Interests

The authors declare no conflict of interest.

Data Availability Statement

The data that support the findings of this study are available in the supplementary material of this article.

Keywords: Electrophilic species · Hydrogenation · Hydrosilylation · Magnesium · Lewis acids

[1] *Lewis Acids in Organic Synthesis* (Ed: H. Yamamoto), Wiley-VCH, Weinheim, Germany **2000**.
[2] G. A. Olah, D. A. Klummp, *Superelectrophiles and Their Chemistry*, John Wiley & Sons Ltd., Hoboken, NJ **2007**.
[3] M. Bochmann, *Coord. Chem. Rev.* **2009**, *253*, 2000–2014.
[4] T. A. Engesser, M. R. Lichtenthaler, M. Schleep, I. Krossing, *Chem. Soc. Rev.* **2016**, *45*, 789–899.
[5] S. Dagorne, D. A. Atwood, *Chem. Rev.* **2008**, *108*, 4037–4071.
[6] S. Schulz, in *Comprehensive Coordination Chemistry III* (Eds.: E.C. Constable, G. Parkin, L. Que Jr) **2021**, Elsevier, Oxford, pp. 66–105.
[7] M. Magre, M. Szewczyk, M. Rueping, *Curr. Opin. Green Sustain. Chem.* **2021**, *32*, 100526.
[8] M. Rauch, S. Ruccolo, G. Parkin, *J. Am. Chem. Soc.* **2017**, *139*, 13264–13267.
[9] M. D. Anker, M. Arrowsmith, P. Bellham, M. S. Hill, G. Kociok-Köhn, D. J. Liptrot, M. F. Mahon, C. Weetman, *Chem. Sci.* **2014**, *5*, 2826–2830.
[10] N. L. Lampland, M. Hovey, D. Mukherjee, A. D. Sadow, *ACS Catal.* **2015**, *5*, 4219–4226.
[11] M. Magre, B. Maity, A. Falconnet, L. Cavallo, M. Rueping, *Angew. Chem. Int. Ed.* **2019**, *58*, 7025–7029.
[12] H. Bauer, M. Alonso, C. Färber, H. Elsen, J. Pahl, A. Causero, G. Ballmann, F. De Proft, S. Harder, *Nat. Catal.* **2018**, *1*, 40–47.
[13] Y. Liang, J. Luo, Y. Diskin-Posner, D. Milstein, *J. Am. Chem. Soc.* **2023**, *145*, 9164–9175.
[14] B. J. Ireland, C. A. Wheaton, P. G. Hayes, *Organometallics* **2010**, *29*, 1079–1084.
[15] Y. Sarazin, M. Schormann, M. Bochmann, *Organometallics* **2004**, *23*, 3296–3302.
[16] M. Rauch, G. Parkin, *J. Am. Chem. Soc.* **2017**, *139*, 18162–18165.
[17] D. Mukherjee, S. Shirase, T. P. Spaniol, K. Mashima, J. Okuda, *Chem. Commun.* **2016**, *52*, 13155–13158.
[18] J. Pahl, A. Friedrich, H. Elsen, S. Harder, *Organometallics* **2018**, *37*, 2901–2909.
[19] J. Pahl, S. Brand, H. Elsen, S. Harder, *Chem. Commun.* **2018**, *54*, 8685–8688.
[20] J. Pahl, T. E. Stennett, M. Volland, D. M. Guldi, S. Harder, *Chem. – Eur. J.* **2019**, *25*, 2025–2034.
[21] N. Adet, D. Specklin, C. Gourlaouen, T. Damiens, B. Jacques, R. J. Wehmschulte, S. Dagorne, *Angew. Chem. Int. Ed.* **2021**, *60*, 2084–2088.
[22] P. Dabringhaus, M. Schorpp, H. Scherer, I. Krossing, *Angew. Chem. Int. Ed.* **2020**, *59*, 22023–22027.
[23] M. Grochowska-Tatarczak, K. Koteras, K. Kazimierczuk, P. J. Malinowski, *Chem. – Eur. J.* **2024**, *30*, e202401322.
[24] I. M. Riddlestone, A. Kraft, J. Schaefer, I. Krossing, *Angew. Chem. Int. Ed.* **2018**, *57*, 13982–14024.
[25] I. Krossing, A. Reisinger, *Coord. Chem. Rev.* **2006**, *250*, 2721–2744.

[26] I. Krossing, H. Brands, R. Feuerhake, S. Koenig, *J. Fluor. Chem.* **2001**, *112*, 83–90.
[27] C. A. Reed, *Acc. Chem. Res.* **1998**, *31*, 133–139.
[28] R. Fischer, D. Walther, P. Gebhardt, H. Görls, *Organometallics* **2000**, *19*, 2532–2540.
[29] K. Tang, A. Du, X. Du, S. Dong, C. Lu, Z. Cui, L. Li, G. Ding, F. Chen, X. Zhou, G. Cui, *Small* **2020**, *16*, 2005424.
[30] P. Sobota, J. Utko, T. Lis, *J. Chem. Soc. Dalton Trans.* **1984**, 2077.
[31] R. J. Wehmschulte, L. Wojtas, *Inorg. Chem.* **2011**, *50*, 11300–11302.
[32] N. Giuseppone, J.-L. Schmitt, L. Allouche, J.-M. Lehn, *Angew. Chem. Int. Ed.* **2008**, *47*, 2235–2239.
[33] R. J. Wehmschulte, B. Bayliss, S. Reed, C. Wesenberg, P. Morgante, R. Peverati, S. Neal, C. D. Chouinard, D. Tolosa, D. R. Powell, *Inorg. Chem.* **2022**, *61*, 7032–7042.
[34] L. O. Müller, D. Himmel, J. Stauffer, G. Steinfeld, J. Slattery, G. Santiso-Quiñones, V. Brecht, I. Krossing, *Angew. Chem. Int. Ed.* **2008**, *47*, 7659–7663.
[35] P. Erdmann, M. Schmitt, L. M. Sigmund, F. Krämer, F. Breher, L. Greb, *Angew. Chem. Int. Ed.* **2024**, *63*, e202403356.
[36] L. Greb, *Chem. – Eur. J.* **2018**, *24*, 17881–17896.
[37] P. R. Markies, O. S. Akkerman, F. Bickelhaupt, W. J. J. Smeets, A. L. Spek, in *Adv. Organomet. Chem*. (Eds.: F.G.A. Stone, R. West), Academic Press, San Diego, USA **1991**, pp. 147–226.
[38] B. Freitag, H. Elsen, J. Pahl, G. Ballmann, A. Herrera, R. Dorta, S. Harder, *Organometallics* **2017**, *36*, 1860–1866.
[39] D. J. Parks, J. M. Blackwell, W. E. Piers, *J. Org. Chem.* **2000**, *65*, 3090–3098.
[40] M. Oestreich, J. Hermeke, J. Mohr, *Chem. Soc. Rev.* **2015**, *44*, 2202–2220.
[41] J. Chen, E. Y.-X. Chen, *Angew. Chem. Int. Ed.* **2015**, *54*, 6842–6846.
[42] L. Garcia, C. Dinoi, M. F. Mahon, L. Maron, M. S. Hill, *Chem. Sci.* **2019**, *10*, 8108–8118.
[43] L. Garcia, M. F. Mahon, M. S. Hill, *Organometallics* **2019**, *38*, 3778–3785.
[44] An initial alkyne activation was recently documented in a Zn-catalyzed alkyne hydrosilylation system: see I. Raz, R. Dobrovetsky, *Chem. – Eur. J.* **2023**, *29*, e202300798.
[45] As DFT-computed, (Figure S81), the release of $[SiEt_3]^+$ from modeled intermediate **G** seems possible.
[46] M. Khandelwal, R. J. Wehmschulte, *Angew. Chem. Int. Ed.* **2012**, *51*, 7323–7326.
[47] X. Xu, C. Gourlaouen, B. Jacques, S. Dagorne, *Organometallics* **2023**, *42*, 2813–2825.
[48] F. J. Fernández-Alvarez, L. A. Oro, *ChemCatChem* **2018**, *10*, 4783–4796.
[49] W. Huadsai, L. Vendier, H. Gorls, L. Magna, S. Bontemps, M. Westerhausen, *Eur. J. Inorg. Chem.* **2024**, *27*, e202400128.
[50] J. Chen, L. Falivene, L. Caporaso, L. Cavallo, E. Y.-X. Chen, *J. Am. Chem. Soc.* **2016**, *138*, 5321–5333.
[51] D. Specklin, F. Hild, C. Fliedel, C. Gourlaouen, L. F. Veiros, S. Dagorne, *Chem. – Eur. J.* **2017**, *23*, 15908–15912.
[52] Y. Liang, U. K. Das, J. Luo, Y. Diskin-Posner, L. Avram, D. Milstein, *J. Am. Chem. Soc.* **2022**, *144*, 19115–19126.
[53] L. J. Hounjet, C. Bannwarth, C. N. Garon, C. B. Caputo, S. Grimme, D. W. Stephan, *Angew. Chem. Int. Ed.* **2013**, *52*, 7492–7495.
[54] D. W. Stephan, *Science* **2016**, *354*, aaf7229–aaf7229.
[55] D. W. Stephan, *J. Am. Chem. Soc.* **2021**, *143*, 20002–20014.

Manuscript received: March 18, 2025
Revised manuscript received: April 12, 2025
Accepted manuscript online: April 17, 2025
Version of record online: April 27, 2025